

Searching for Long Strings in CMB Maps

L. Perivolaropoulos

*Department of Physics, University of Crete
P.O.Box 2208, 710 03 Heraklion, Crete; Greece
e-mail: leandros@physics.uh.gr
(March 24, 2018)*

Using analytical methods and Monte Carlo simulations, we analyze new statistics designed to detect isolated step-like discontinuities which are coherent over large areas of Cosmic Microwave Background (CMB) pixel maps. Such coherent temperature discontinuities are predicted by the *Kaiser-Stebbins* effect to form due to long cosmic strings present in our present horizon. The background of the coherent step-like seed is assumed to be a scale invariant Gaussian random field which could have been produced by a superposition of seeds on smaller scales and/or by inflationary quantum fluctuations. We find that the proposed statistics can detect the presence of a coherent discontinuity at a sensitivity level almost an order of magnitude better compared to more conventional statistics like the skewness or the kurtosis.

I. INTRODUCTION

The major progress achieved during the past 15 years in both theory and cosmological observations has turned the search for the origin of cosmic structure into one of the most exciting fields of scientific research. Despite the severe constraints imposed by detailed observational data on theories for structure formation the central question remains open: *What is the origin of primordial fluctuations that gave rise to structure in the universe?* Two classes of theories attempting to answer this question have emerged during the past twenty years and have managed to survive through the observational constraints with only minor adjustments.

According to the first class, primordial fluctuations are produced by quantum fluctuations of a linearly coupled scalar field during a period of inflation [1]. These fluctuations are subsequently expected to become classical and provide the progenitors of structure in the universe. Because of the extremely small linear coupling of the scalar field, needed to preserve the observed large scale homogeneity, the inflationary perturbations are expected by the central limit theorem, to obey Gaussian statistics. This is not the case for the second class of theories.

According to the second class of theories [2], primordial perturbations are provided by *seeds* of trapped energy density produced during symmetry breaking phase transitions in the early universe. Such symmetry break-

ing is predicted by Grand Unified Theories (GUT's) to occur at early times as the universe cools and expands. The geometry of the produced seeds, known as *topological defects* is determined by the topology of the vacuum manifold of the physically realized GUT. Thus the defects may be pointlike (monopoles), linelike (cosmic strings), planar (domain walls) or collapsing pointlike (textures).

The cosmic string theory [3] for structure formation is the oldest and (together with textures [4]) best studied theory of the topological defect class. By fixing its single free parameter $G\mu$ (μ is the *effective* mass per unit length of the wiggly string G is Newtons constant and we have used units with $c = 1$) to a value consistent with microphysical requirements coming from GUT's ($G\mu \simeq 10^{-6}$), the theory is consistent with the noise in pulsar signal arrival times assuming that the noise is due to gravitational radiation emitted by the defect network [5]. It may automatically account for large scale filaments and sheets [6], galaxy formation at epochs $z \sim 2 - 3$ [7] and galactic magnetic fields [8]. It can also provide large scale peculiar velocities [9] and is consistent with the amplitude, spectral index [10] and the statistics [11] of the cosmic microwave background (CMB) anisotropies measured by the COBE collaboration [12] on large angular scales ($\theta \sim 10^\circ$). Other planned CMB experiments [13] of equally high quality but on smaller angular scales are expected to provide a wealth of information within the next few years.

The CMB observations provide a valuable direct probe for identifying signatures of cosmic strings. The main mechanism by which strings can produce CMB fluctuations on angular scales larger than 1-2 degrees has been well studied both analytically [14] and using numerical simulations [10] and is known as the *Kaiser-Stebbins effect* [15]. According to this effect, moving long strings present between the time of recombination t_{rec} and the present time t_0 , produce step-like temperature discontinuities between photons that reach the observer through opposite sides of the string. These discontinuities are due to the peculiar nature of the spacetime around a long string which even though is *locally* flat, *globally* has the geometry of a cone with deficit angle $8\pi G\mu$. The magnitude of the discontinuity is proportional to the deficit angle, to the string velocity v_s and depends on the relative orientation between the unit vector along the string \hat{s} and the unit photon wave-vector \hat{k} . It is given by [14]

$$\frac{\delta T}{T} = \pm 4\pi G\mu v_s \gamma_s \hat{k} \cdot (\hat{v}_s \times \hat{s}) \quad (1)$$

where γ_s is the relativistic Lorentz factor and the sign changes when the string is crossed. The angular scale over which this discontinuity persists is given by the radius of curvature of the string which according to simulations [16] is approximately equal to the horizon scale. The growth of the horizon from t_{rec} to t_0 results in a superposition of a large number of step-like temperature seeds of all sizes starting from about 2° (the angular size of the horizon at t_{rec}) to about 180° (the present horizon scale). By the central limit theorem this large number of superposed seeds results in a pattern of fluctuations that obeys Gaussian statistics. Thus the probability distribution for the temperature of each pixel of a CMB map with resolution larger than about $1^\circ - 2^\circ$ is a Gaussian [17]. It has therefore been considered to be impossible to distinguish structure formation models based on cosmic strings from corresponding models based on inflation, using CMB maps with resolution angle larger than $1^\circ - 2^\circ$. Theoretical studies have therefore focused on identifying the statistical signatures of cosmic strings on angular scales less than 1° [11] where the number of superposed seeds is smaller and therefore the non-Gaussian character of fluctuations is expected to be stronger ¹

These efforts however have been faced with the complicated and model dependent physical processes occurring on small angular scales. Such effects include isolated foreground point sources, recombination physics, string properties on small scales (kinks, loops etc) which require detailed simulations of both the string network and the cosmic background, in order to be properly taken into account. Even though there are preliminary efforts for such detailed simulations [17], it has become clear that it will take some time before theory and experiments on angular scales less than a few arcmin reach accuracy levels leading to detectable non-Gaussian string signatures.

An alternative approach to the problem is instead of focusing on small scales where the number of superposed seeds is small, to focus on larger angular scales where despite the large number of superposed seeds there is also coherence of induced fluctuations on large angular scales. Fluctuations on these scales may be viewed as a superposition of a Gaussian scale invariant background coming mainly from small scale seeds plus a small number of step-like discontinuities which are coherent and persist on angular scales of order 100° . These are produced by long strings present in our present horizon. *Our goal is to find*

a statistic optimized to detect this large scale coherence and use it to find the minimum amplitude of a coherent discontinuity that can be detected at the $1\sigma - 2\sigma$ level relatively to a given scale invariant or noise dominated Gaussian background. Such a statistic is equally effective on *any* angular resolution scale and its effectiveness is only diminished as the number of pixels of the CMB map is reduced or the noise is increased. The statistical variable we focus on, in sections 2 and 3 is the Sample Mean Difference (SMD) of temperatures between large neighbouring sectors of a CMB map. These sectors are separated by a random straight line in two dimensional maps or by a random point in one dimensional maps. The union of the two sectors gives back the complete map. We show that the statistics of the SMD variable are much more sensitive in detecting the presence of a coherent step-like seed than conventional statistics like the skewness or the kurtosis.

We also discuss an alternative statistic, the Maximum Sample Difference that is more sensitive in certain cases but less robust than the SMD. This statistic is based on finding the maximum from a large sample of temperature differences between large neighbouring sectors of CMB maps. We show that for noise dominated data the MSD statistic is even more sensitive than the SMD statistic. However, this sensitivity gets rapidly reduced when significant correlations are introduced in the underlying Gaussian data. Thus the MSD statistic is more sensitive but less robust compared to the SMD statistic.

The structure of this paper is the following: In the next section titled 'Sample Mean Difference' we study analytically the statistics of the SMD variable and show that its average value is a sensitive quantity in detecting the presence of a randomly positioned step-function on top of a Gaussian map. We then compare with the sensitivity of the statistics *skewness* and *kurtosis*. We find that the sensitivity of the SMD statistic is significantly superior to that of skewness and kurtosis in detecting the step function. These analytical results are shown for the case of one-dimensional maps but the extension to the case of two dimensional maps is straightforward.

In the third section titled 'Monte Carlo Simulations' we perform Monte Carlo simulations of Gaussian maps with and without step-like discontinuities in one and two dimensions. Applying the statistics skewness, kurtosis and average of SMD on these maps we verify the analytical results of section 2 and find the minimum step-function amplitude that is detectable by the average SMD statistic. In section 4 we show both analytically and numerically that the MSD statistic can be significantly more sensitive and accurate even compared to the SMD statistic when applied to noise dominated data.

Finally in section 5 we conclude, summarise and discuss the prospect of applying the average of SMD statistic

¹The non-Gaussian features for texture maps are stronger than those of cosmic strings mainly because of the generically smaller number of textures per horizon volume [18].

and the MSD statistic to presently available CMB maps including the COBE data. That analysis is currently in progress [19], and will be presented separately.

II. SAMPLE MEAN DIFFERENCE

Consider an one dimensional array of n pixel variables x_n . Let these variables be initially distributed according to a standardised Gaussian probability distribution. Consider now a step-function of amplitude 2α superposed so that the discontinuity is between pixels i_0 and $i_0 + 1$ (Fig. 1). The new probability distribution for a random pixel variable x is

$$P(x) = \frac{f}{\sqrt{2\pi}} e^{-\frac{(x-\alpha)^2}{2}} + \frac{1-f}{\sqrt{2\pi}} e^{-\frac{(x+\alpha)^2}{2}} \quad (2)$$

where $f = \frac{i_0}{n}$. We are looking for a statistic that will optimally distinguish between a Gaussian array with a superposed step-function and a Gaussian array without one. The obvious statistics to try first are the moments of the distribution (2) with $\alpha = 0$ and $\alpha \neq 0$.²

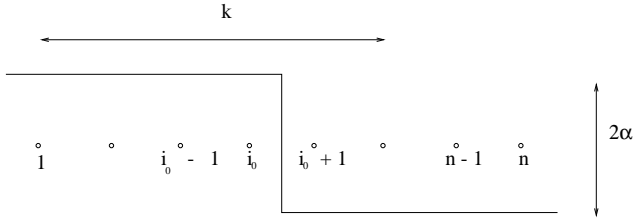


Figure 1: A large scale coherent step-function discontinuity superposed on a one dimensional pixel map.

The moment generating function corresponding to (2) is:

$$M(t) = f e^{at + \frac{t^2}{2}} + (1-f) e^{-at + \frac{t^2}{2}} \quad (3)$$

The mean $\mu(\alpha, f)$, variance $\sigma^2(\alpha, f)$, skewness $s(\alpha, f)$ and kurtosis $k(\alpha, f)$ can be obtained in a straightforward way by proper differentiation of $M(t)$ as follows:

$$\begin{aligned} \mu(\alpha, f) &\equiv \langle X \rangle = \alpha f - \alpha(1-f) \\ \sigma^2(\alpha, f) &\equiv \langle (x-\mu)^2 \rangle = 1 + 4\alpha^2 f(1-f) \\ s(\alpha, f) &\equiv \frac{\langle (x-\mu)^3 \rangle}{\sigma^3} = \frac{8\alpha^3 f(1-3f+2f^2)}{(1+4\alpha^2 f(1-f))^{3/2}} \end{aligned}$$

$$\begin{aligned} k(\alpha, f) &\equiv \frac{\langle (x-\mu)^4 \rangle}{\sigma^4} \\ &= \frac{3 + 8\alpha^2 f(3 + 2\alpha^2 - 3f^2 - 8\alpha^2 f + 12\alpha^2 f^2 - 6\alpha^2 f^3)}{(1 + 4\alpha^2 f(1-f))^4} \end{aligned}$$

For $\alpha = 0$ we obtain the Gaussian values for the skewness and the kurtosis $s(0, f) = 0$, $k(0, f) = 3$ as expected. For $\alpha \neq 0$ the moments deviate from the Gaussian values. In order to find the minimum value of α for which the moments can distinguish between a Gaussian pattern and a Gaussian+Step pattern we must compare the deviation of moments from their Gaussian values with the standard deviation of the sample moments. The mean values of the skewness and the kurtosis are easily obtained by integrating with respect to f from 0 to 1 i.e. assuming that it is equally probable for the step-function to be superposed at any point of the lattice.

$$\bar{s}(\alpha) = \langle s(\alpha, f) \rangle = \int_0^1 df s(\alpha, f) = 0 \quad (4)$$

$$\bar{k}(\alpha) = \langle k(\alpha, f) \rangle = \int_0^1 df k(\alpha, f) \quad (5)$$

These values are to be compared with the standard deviations of the moments, obtained as follows: The variance of the skewness over several n -pixel array realizations with fixed f and α is

$$\Delta s^2(\alpha, f) = \langle (\hat{s} - s)^2 \rangle \quad (6)$$

where $\hat{s} \equiv \frac{s_1 + \dots + s_n}{n}$ is the sample skewness from a given pixel array realization, s is the actual skewness (for $n \rightarrow \infty$) and $s_i \equiv \frac{(x_i - \mu)^3}{\sigma^3}$. Now

$$\langle \hat{s} \rangle = \frac{n \langle s_1 \rangle}{n} = \langle s_1 \rangle = s \quad (7)$$

Also

$$\langle \hat{s}^2 \rangle = \frac{1}{n} \langle s_j^2 \rangle + (1 - \frac{1}{n}) \langle s_j \rangle^2 \quad (8)$$

where j any pixel number ($j \in [1, n]$). Thus

$$\Delta s^2(\alpha, f) = \frac{1}{n} (\langle s_j^2 \rangle - \langle s_j \rangle^2) \quad (9)$$

Similarly for the variance of the sample kurtosis we have

$$\Delta k^2(\alpha, f) = \frac{1}{n} (\langle k_j^2 \rangle - \langle k_j \rangle^2) \quad (10)$$

²With no loss of generality we may assume α positive or 0 because from the statistical point of view there is $\alpha \leftrightarrow -\alpha$ symmetry.

with $k_j = \frac{1}{\sigma^4}(x_j - \mu)^4$ and $\langle k_j^2 \rangle = \frac{1}{\sigma^8} \langle (x_j - \mu)^8 \rangle$. It is straightforward to obtain all the above moments by differentiating the generating functional and using

$$\langle x_j^n \rangle = \frac{d^n M}{dt^n} \Big|_{t=0} \quad (11)$$

Now the minimum value α_{min} of α detectable at 1σ level is obtained from the equations

$$\int_0^1 df [s(\alpha_{min}, f) - \Delta s(\alpha_{min}, f)] = 0 \quad (12)$$

$$\int_0^1 df [(k(\alpha_{min}, f) - 3) - \Delta k(\alpha_{min}, f)] = 0 \quad (13)$$

Since (from eq. (4)) $\bar{s}(\alpha) = 0$ which is equal to the Gaussian value, the skewness can only be used to detect a step function by comparing the standard deviation $\Delta \bar{s}$ for $\alpha = 0$ and $\alpha \neq 0$. By demanding $\Delta \bar{s}(\alpha_{min}) \leq 2\Delta \bar{s}(\alpha = 0)$ we obtain $\alpha_{min} \leq 2.5$. This result is independent of the number of pixels n . For the kurtosis we obtain from eqs. (10, 13) $\alpha_{min} \simeq 4$ for $n = 10^3$ while for $\alpha_{min} = 0.5$, $n \simeq 10^6$ is required.

Using the alternative test i.e. demanding $\Delta \bar{k}(\alpha_{min}) \geq 2\Delta \bar{k}(\alpha = 0)$ we obtain $\alpha \geq 2$ and this result is independent of the number of pixels n as in the case of skewness. Thus for the usual pixel maps where n is up to $O(1000)$ the kurtosis is not able to detect a step function with $|\alpha| \leq 2$ at the 1σ level.³ This result remains unchanged for other statistical variables defined by *local* linear combinations of pixels (e.g. differences of neighbouring pixel variables [11]) since the effect of a single discontinuity remains negligible if the long range coherence is not taken into account.

For CMB temperature maps with $(\frac{\delta T}{T})_{rms} \simeq 2 \times 10^{-5}$ the detectable value of $G\mu$ is

$$\begin{aligned} \alpha &\equiv 4\pi G\mu(v_s \gamma_s) \cos \theta > 4 \times 10^{-5} \\ &\Rightarrow G\mu(v_s \gamma_s) \cos \theta \gtrsim 4 \times 10^{-6} \end{aligned} \quad (14)$$

where θ is an angle obtained from the relative orientation of the string with respect to the observer. According to simulations $\langle v_s \gamma_s \rangle_{rms} \simeq 0.2$ and for $G\mu < 2 \times 10^{-5}$ the detection of the Kaiser-Stebbins effect using statistics based on skewness and kurtosis is not possible. This excluded range however includes all the cosmologically interesting values of $G\mu$.

It is therefore important to look for alternative statistical variables that are more sensitive in detecting the

presence of coherent discontinuities superposed on Gaussian maps. It will be shown that the Sample Mean Difference (SMD) is such a statistical variable. A similar and even more effective statistic, the Maximum Sample Difference will be discussed in section IV.

Consider a pixel array (Fig. 1) of n pixel Gaussian random variables X_j with a step function covering the whole array, superposed such that the discontinuity is located just after pixel i_0 . To every pixel k of the array we may associate the random variable Y_k defined as the difference between the mean value of the pixels 1 through k minus the mean value of the pixels $k+1$ through n . It is straightforward to show that

$$Y_k = \Delta \bar{X}_k + 2\alpha \frac{n - i_0}{n - k} \quad k \in [1, i_0] \quad (15)$$

$$Y_k = \Delta \bar{X}_k + 2\alpha \frac{i_0}{k} \quad k \in [i_0, n - 1] \quad (16)$$

where $\Delta \bar{X}_k \equiv \frac{1}{k} \sum_{j=1}^k X_j - \frac{1}{n-k} \sum_{j=k+1}^n X_j$. Thus we have constructed a new array Y_k , ($k = 1, \dots, n-1$) from the sample mean differences (SMD) of the original array. We will focus on the average value Z of the SMD defined as:

$$Z = \frac{1}{n-1} \sum_{k=1}^{n-1} Y_k \quad (17)$$

Using eqs. (15-17) we obtain

$$Z = \frac{1}{n-1} \left[\sum_{k=1}^{n-1} \Delta \bar{X}_k + 2\alpha \left(\sum_{k=1}^{i_0} \frac{1 - i_0/n}{1 - k/n} + \sum_{k=i_0+1}^{n-1} \frac{i_0/n}{k/n} \right) \right] \quad (18)$$

With the definitions $f \equiv i_0/n$ and $\xi \equiv k/n$ and the assumption $n \gg 1$ we obtain:

$$Z = \frac{1}{n-1} \sum_{k=1}^{n-1} \Delta \bar{X}_k - 2\alpha [(1-f) \ln(1-f) + f \ln f] \quad (19)$$

Thus the mean of Z over many realizations of the array is

$$\langle Z \rangle = \frac{1}{n-1} \sum_{k=1}^{n-1} \langle \Delta \bar{X}_k \rangle - 4\alpha \left[\int_0^1 df f \ln f \right] = \alpha \quad (20)$$

The variance of Z is due both to the underlying Gaussian map and to the variation of $f = i_0/n$ (assuming α fixed). The variance due to the gaussian background is

³As in all cases discussed in this paper α is measured in units of standard deviation (rms) of the underlying Gaussian map.

$$\sigma_{1,Z}^2 = \frac{1}{(n-1)^2} \sum_{k=1}^{n-1} \left(\frac{1}{k} + \frac{1}{n-k} \right) \simeq \epsilon \int_{\epsilon}^{1-\epsilon} \frac{d\xi}{\xi(1-\xi)} \quad (21)$$

where $\epsilon = O(\frac{1}{n})$, $\xi = k/n$, $n \gg 1$ and we have used the fact that the variance of the sample mean of a standardized Gaussian population with size j is $\frac{1}{j}$. Now from eq. (21) we obtain

$$\sigma_{1,Z}^2 \simeq -\epsilon \ln \epsilon^2 \simeq \frac{2 \ln n}{n} \quad (22)$$

The variance of the f -dependent part of Z is

$$\sigma_{2,Z}^2 = \langle Z_2^2 \rangle - \langle Z_2 \rangle^2 \quad (23)$$

where $Z_2 \equiv -2\alpha[(1-f) \ln(1-f) + f \ln f]$. From eq. (20) we have $\langle Z_2 \rangle = \alpha$ and $\langle Z_2^2 \rangle$ is easily obtained as

$$\langle Z_2^2 \rangle = \int_0^1 df Z_2^2(f) \simeq \frac{4}{3} \alpha^2 \quad (24)$$

Thus

$$\sigma_Z^2 \equiv \sigma_{1,Z}^2 + \sigma_{2,Z}^2 = \frac{2 \ln n}{n} + \frac{1}{3} \alpha^2 \quad (25)$$

In order to be able to distinguish between a Gaussian+Step map and a purely Gaussian one, at the $m\sigma$ level we demand that

$$|Z_{\alpha \neq 0} - Z_{\alpha=0}| \geq m \sigma_{1Z} \quad (26)$$

where we have used the variance σ_{1Z} of a given realization. This implies that the minimum value of α , α_{min} that can be detected using this test is

$$\alpha_{min} = m \left(\frac{2 \ln n}{n} \right)^{1/2} \quad (27)$$

and for $n = O(10^3)$ we obtain $\alpha_{min} \simeq m \cdot 0.2$ which for $m = 1$ is about *an order of magnitude improvement* over the corresponding sensitivity of tests based on the moments skewness and kurtosis. The reason for this significant improvement is the fact that the SMD statistical variable picks up the *coherence* properties introduced by the step function on the Gaussian map. The moments on the other hand pick up only local properties of the pixels and do not amplify the long range coherence of the step-like discontinuity.

Our analysis so far has assumed that the Gaussian variables X_j are independent and that the only correlation is introduced by the superposed step-function. In a realistic setup however the underlying Gaussian map

will be scale invariant and thus there will be correlations among the pixels. These correlations will also be affected by the instrument noise. In addition, our analysis has been limited so far to one dimensional maps while most CMB experiments are now obtaining two-dimensional maps. In order to take all these effects into account we need to apply the statistics of the SMD variable onto maps constructed by Monte Carlo simulations. This is the focus of the following section.

III. MONTE-CARLO SIMULATIONS

We start by constructing an array of n Gaussian random variables X_j , $j = 1, \dots, n$ with a power spectrum $P(k) = k^{-m}$. Thus the values X_j associated with the pixel j are obtained as the Fourier transform of a function $g(k)$ ($k = 1, \dots, n$) with the following properties:

- For each k , the amplitude $|g(k)|$ is an independent Gaussian random variable with 0 mean and variance $P(k) = 1/k^m$.
- The phase θ_k of each Fourier component $g(k)$ is an independent random variable in the range $[0, 2\pi]$ with uniform probability distribution $P(\theta_k) = \frac{1}{2\pi}$.
- The Fourier components are related by complex conjugation relations needed to give a *real* variable X_j .

The discrete Fourier transform definition used is

$$X_j = \frac{1}{\sqrt{n}} \sum_{k=1}^n g(k) e^{2\pi i (k-1)(j-1)/n} \quad (28)$$

and the numerical programming was implemented using *Mathematica* [20]. The array X_j obtained in the way described above is then standardized to the array X_j^s , with

$$X_j^s \equiv \frac{(X_j - \mu)}{\sigma} \quad (29)$$

where μ and σ^2 are the sample mean and sample variance for the realization of the array X_j . A new array X_j' is then constructed by superposing to the array X_j^s a step function of amplitude 2α with discontinuity at a random point i_0 . The array X_j' is thus obtained as

$$X_j' = X_j^s + \alpha \frac{j - i_0}{|j - i_0|}, \quad j = 1, \dots, n \quad (30)$$

Next we apply the statistics discussed in the previous section to several realizations of the arrays X_j^s and X_j'

in an effort to find the most sensitive statistic that can distinguish among them. Our goal is to also find the minimum value of α that can be distinguished by that statistic at the 1σ level, thus testing the analytical results of the previous section.

We have used a lattice with 2000 pixels and a scale invariant power spectrum which for one-dimensional data is $P(k) = k^{-1}$. In Table 1 we show the results for the skewness, the kurtosis and the average SMD for the X_j arrays, with $\alpha = 0, 0.25, 0.50$ and 1.0 . The SMD average was obtained as in section 2 by first constructing the array of sample mean differences and then obtaining its average value, predicted to be equal to α by the analytical study of section 2.

These statistics were applied to 50 random realizations of the array X_j^s . The mean values of the statistics considered with their 1σ standard deviations obtained over these 50 realizations are shown in the following Table 1.

Table 1: A comparison of the effectiveness of the statistics considered, in detecting the presence of a coherent step discontinuity with amplitude 2α relative to the standard deviation of the underlying scale invariant Gaussian map.

α	Skewness	Kurtosis	—SMD Average—
0.00	0.01 ± 0.11	2.97 ± 0.19	0.02 ± 0.31
0.25	0.01 ± 0.11	2.95 ± 0.20	0.25 ± 0.33
0.50	0.02 ± 0.11	2.88 ± 0.21	0.48 ± 0.38
1.00	0.03 ± 0.20	2.82 ± 0.32	0.98 ± 0.48

The analytical prediction of section 2 for the SMD average value α is in good agreement with the results of the Monte Carlo simulations. The standard deviation of this result is not in such a good agreement with the analytical prediction because the assumption of complete independence among pixels made by the analytical treatment is not realized in the Monte Carlo simulations. here a scale invariant spectrum was considered and thus there was a non-trivial correlation among the pixels of the arrays.

A simple way to further improve the sensitivity of the SMD statistical variable is to ignore a number l of boundary pixels of the SMD array, thus constructing its average using the Sample Mean Differences of pixels $l+1, \dots, n-l$. From eq (21), the variance of the SMD for these pixels is significantly lower than the corresponding variance of the $2l$ pixels close to the boundaries. In addition, if the step is located within the central $n - 2l$ pixels the SMD average may be shown to be larger than α thus further amplifying the step signature. For $l = 150$ the variance of the SMD average *is reduced* by about 20% while the SMD average is *increased* by about 20% thus allowing the detection of steps as low as $\alpha = 0.25$ at the 1σ level.

The price to pay for this sensitivity improvement is the reduction of the effective pixel area where the search for steps is made.

We have also used the SMD statistical variable for non-scale invariant power spectra and found that it works better for $P(k) = k^{-m}$ with $0 \leq m < 1$ than for $m > 1$. This is to be expected because large values of m imply larger correlations among pixels which in turn leads to a smaller number of effectively independent pixels and thus a larger value for the variance of the SMD average.

It is straightforward to generalize the one dimensional Monte Carlo simulations to two dimensions. In that case we use the two-dimensional discrete Fourier transform as an approximation to an expansion to spherical harmonics. This approximation is good for small area maps of the celestial sphere. We used the following definition of the two dimensional discrete Fourier transform.

$$X(i, j) = \frac{1}{n} \sum_{k_1, k_2=1}^n g(k_1, k_2) e^{2\pi i[(i-1)(k_1-1) + (j-1)(k_2-1)]/n} \quad (31)$$

referring to a $n \times n$ square lattice. In order to construct the background of scale invariant Gaussian fluctuations we used $g(k_1, k_2)$ as a complex random variable. For scale invariance, the amplitude of $g(k_1, k_2)$ was obtained from a Gaussian probability distribution with 0 mean and variance

$$\sigma^2(k_1, k_2) = P(k_1, k_2) = \frac{1}{k_1^2 + k_2^2} \quad (32)$$

The corresponding phase θ_{k_1, k_2} for the (k_1, k_2) mode was also determined randomly from a uniform probability distribution $P(\theta_{k_1, k_2}) = \frac{1}{2\pi}$ in order to secure Gaussianity for the map $X(i, j)$.

The corresponding map with a superposed coherent step discontinuity was obtained from the standardized Gaussian map $X^s(i, j)$ as

$$X'(i, j) = X^s(i, j) + \alpha \frac{j - a i - b}{|j - a i - b|} \quad (33)$$

where

$$a = \frac{y_2 - y_1}{x_2 - x_1} \quad (34)$$

$$b = y_1 - a x_1 \quad (35)$$

i.e. the line of step discontinuity $j = a i + b$ is determined by the two random points (x_1, y_1) and (x_2, y_2) of the map $X(i, j)$. The skewness and kurtosis of the two maps are obtained in the usual way. For example for the standardized Gaussian map $X^s(i, j)$ we have

$$s = \frac{1}{n^2} \sum_{i,j}^n X^s(i, j)^3 \quad (36)$$

$$k = \frac{1}{n^2} \sum_{i,j}^n X^s(i, j)^4 \quad (37)$$

The SMD statistical variable is obtained by considering a set of random straight lines bisecting the map and for each line taking the difference of the sample means from the two parts of the map. For example consider a line defined by the random points (x_1, y_1) and (x_2, y_2) of the map. The line equation is $j = a i + b$ with a, b obtained from eqs. (34) and (35). The SMD obtained from this line is

$$SMD = \frac{S_1}{n_1} - \frac{S_2}{n_2} \quad (38)$$

where

$$S_1 = \sum_{i=1}^n \sum_{j=Max[(a i+b), 1]}^n X^s(i, j) \quad (39)$$

$$S_2 = \sum_{i=1}^n \sum_{j=1}^{Min[(a i+b), n]} X^s(i, j) \quad (40)$$

and n_1, n_2 are the corresponding numbers of terms in the sums. For a Step+Gaussian map, the index s get replaced by $'$.

The average and variance of the SMD is obtained by averaging over a large number of random test lines (a, b) and a large number of map realizations. The results of the application of the three statistics (skewness, kurtosis and SMD average) on 30×30 scale invariant Gaussian maps for various values of step amplitudes α are shown in Table 2. Uncorrelated Gaussian noise was also superposed on the signal with signal to noise ratio 2.0. The random points defining the test lines were excluded from the outermost three rows and columns of the maps thus reducing somewhat the variance of the SMD average.

Table 2: A comparison of the effectiveness of the statistics considered in two dimensional maps. The signal to noise ratio was 2.0. Points defining the line discontinuities were excluded from the three outermost rows and columns of the maps.

α	Skewness	Kurtosis	SMD Average
0.00	0.04 ± 0.13	3.00 ± 0.20	0.01 ± 0.03
0.25	0.02 ± 0.08	2.97 ± 0.13	0.14 ± 0.09
0.50	0.05 ± 0.14	2.91 ± 0.24	0.34 ± 0.19
1.00	0.02 ± 0.24	2.95 ± 0.30	0.56 ± 0.31

The results of Table 4 are in qualitative agreement with those of Table 1 and with the analytical results valid

for the one dimensional maps. Clearly the details of the one dimensional analysis are not valid in the two dimensional case and so the agreement can not be quantitative. The results still indicate however that the SMD statistic is significantly more sensitive compared to conventional statistics for the detection of coherent discontinuities on CMB maps. This statistic can detect coherent discontinuities with minimum amplitude $\alpha_{min} \simeq 0.5$ at the 1σ to 2σ level where α is the amplitude relative to the standard deviation of the underlying scale invariant Gaussian map.

IV. MAXIMUM SAMPLE DIFFERENCE

An alternative statistic that can be significantly more sensitive than the SMD in certain cases is the *Maximum Sample Difference* (MSD). For an one dimensional set of data the MSD statistical variable $Max(r_k)$ is defined as

$$Max(r_k) = Max\left(\frac{Y_k}{\sigma(Y_k)}\right) \quad (41)$$

where Y_k is given by equations (15), (16) and $\sigma(Y_k)$ is the standard deviation of Y_k given by

$$\sigma(Y_k) = \sqrt{\frac{1}{k} + \frac{1}{n-k}} \quad (42)$$

The variable r_k has variance unity and mean

$$\mu(\alpha, n, k, i_0) = 2\alpha \frac{(n - i_0)/(n - k)}{\sigma(k)} \quad 1 < k < i_0 \quad (43)$$

$$\mu(\alpha, n, k, i_0) = 2\alpha \frac{i_0/k}{\sigma(k)} \quad i_0 < k < n - 1 \quad (44)$$

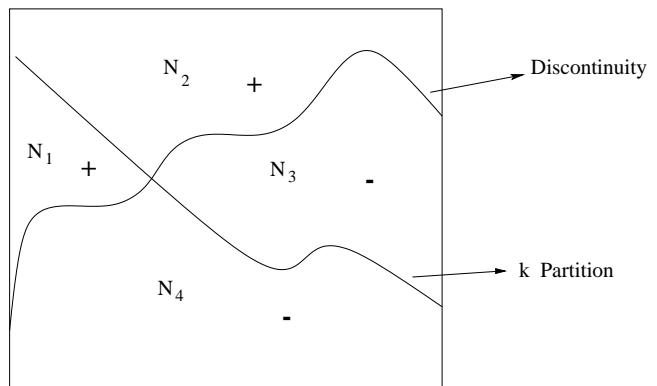


Figure 2: The sample division described by k and the coherent discontinuity location described by i_0 divide the 2d pixel-map into four parts with corresponding number of pixels $N_i, i = 1, \dots, 4$.

For two dimensional datasets the index \bar{k} labels *partitions* by which the two dimensional pixel-surface is divided in two parts. In the Monte-Carlo simulations studied here we have considered only map divisions represented by straight lines. It is straightforward however to generalize this to other types of divisions. In the 2d case $Y_{\bar{k}}$ is generalized to the expression given in equation (38). Let the set of parameters \bar{i}_0 describe the location and shape of the coherent discontinuity in the 2d map (in the simplest case of a straight line discontinuity \bar{i}_0 represents only two numbers). Let also the set of parameters \bar{k} describe the location of the sample division of the 2d map. With the sample division described by \bar{k} and the coherent discontinuity location described by \bar{i}_0 the 2d pixel-map is divided into four parts with corresponding number of pixels N_i , $i = 1, \dots, 4$ (Figure 2). For simplicity, hereafter we will omit the bar in \bar{i}_0 and \bar{k} thus using the same notation as in the 1d case.

Thus

$$Y_k = \frac{S_1}{N_1 + N_4} - \frac{S_2}{N_2 + N_3} \quad (45)$$

$$\sigma(Y_k) = \sqrt{\frac{1}{N_1 + N_4} + \frac{1}{N_2 + N_3}} \quad (46)$$

with

$$r_k \equiv \frac{Y_k}{\sigma(Y_k)} = u_k + 2\alpha \frac{w_k(i_0)}{\sigma(Y_k)} \quad (47)$$

where $u_k \equiv \frac{\Delta \bar{x}_k}{\sigma(Y_k)}$ is a standardized Gaussian random variable and

$$w_k(i_0) = \frac{1}{2} \left(\frac{N_1 - N_4}{N_1 + N_4} - \frac{N_2 - N_3}{N_2 + N_3} \right) \quad (48)$$

Define now $\alpha_{eff} = \alpha w_k(i_0)$. Clearly when the partition k coincides with the discontinuity i_0 ($N_4 \rightarrow 0$ and $N_2 \rightarrow 0$) we have $\alpha_{eff} \rightarrow \alpha$. Otherwise $|\alpha_{eff}| < |\alpha|$. The statistical variable r_k is Gaussian with variance unity and mean

$$\langle r_k \rangle = \frac{2\alpha_{eff}}{\sigma(Y_k)} \leq \frac{2\alpha}{\sigma(Y_k)} \quad (49)$$

The $Max(|r_k|)$ after n trials (partitions) is therefore a sensitive function of α_{eff} (in the limit where we take *all* possible partitions we will also have a partition with $\alpha_{eff} \rightarrow \alpha$).

Now assume that after n trials (partitions) we found $Max(|r_k|) = V_0 > 0$. Since the variable u_k of equation (53) is standardized Gaussian the probability $p_>(V_0)$ at *each trial* that we obtain a value V_0 or larger for $|r_k|$ is

$$p_>(V_0, \alpha_{eff}) = \frac{1}{\sqrt{2\pi}} \int_{|V_0|}^{\infty} dr_k e^{-\frac{(r_k - (2\alpha_{eff}/\sigma(Y_k)))^2}{2}} + \frac{1}{\sqrt{2\pi}} \int_{-|V_0|}^{-\infty} dr_k e^{-\frac{(r_k - (2\alpha_{eff}/\sigma(Y_k)))^2}{2}} \quad (50)$$

Using the binomial distribution we find the probability for x values of r_k above V_0 after n partitions to be

$$P_x(n, V_0, \alpha_{eff}) = \frac{n!}{x!(n-x)!} p_>(V_0, \alpha_{eff})^x (1 - p_>(V_0, \alpha_{eff}))^{n-x} \quad (51)$$

In our case we have *only one* occurrence of V_0 (since it is maximum) and the probability for this to happen is $P_1(n, V_0, \alpha_{eff})$. Thus, from a 2d pixel-map we can measure V_0 (the maximum of r_k , n (the number of divisions used in the test) and $\sigma(Y_{k_0})$ (for the partition k_0 that corresponds to V_0)). With this input we obtain the probability distribution $P_1(\alpha_{eff})$ given n , V_0 and $\sigma(Y_{k_0})$. For example assume that we measured V_0 with 100 divisions ($n = 100$) in a 30×30 pixel map. A reasonable value of $\sigma(Y_{k_0})$ (to be obtained exactly from the data) is

$$\sigma(Y_{k_0}) = \sqrt{\frac{1}{N_1 + N_4} - \frac{1}{N_2 + N_3}} \simeq \frac{2}{\sqrt{N}} \simeq 0.07 \quad (52)$$

Given n , V_0 and $\sigma(Y_{k_0})$, the probability distribution $P_1(\alpha_{eff})$ is an even function of α_{eff} , completely determined and has maxima $P_1(\alpha_{eff}^{max})$ at $\pm \alpha_{eff}^{max}$. For larger V_0 we expect larger α_{eff}^{max} .

For example, it may be easily verified using equation (57) and the package *M* athematica that with $n = 100$ we have $|\alpha_{eff}^{max}| = 0$ for $V \leq V_0^{crit} \simeq 2.5$. In general, given n , V_0 and $\sigma(Y_{k_0})$, we can determine the probability distribution for α_{eff} and therefore the most probable value of α_{eff} (a lower bound on α) can be found. This most probable value is α_{eff}^{max} and the corresponding probability is $P_1(\alpha_{eff}^{max})$. We also find the probability that there is no coherent discontinuity on the map as $P_1(\alpha_{eff} = 0)$ (for $V_0 < V_0^{crit}$ it is most probable that there is no coherent discontinuity on the map).

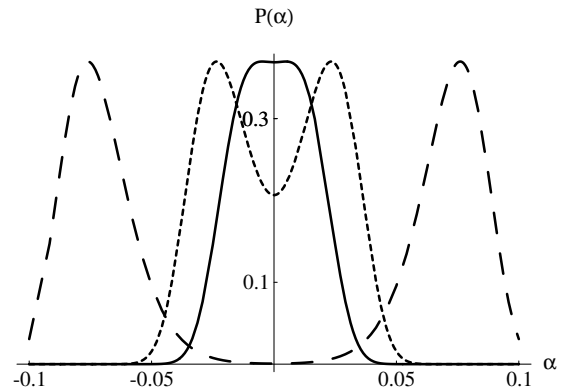


Figure 3: plot of $P_1(\alpha_{eff})$ for $V_0 = 2.6$ (continuous line), $V_0 = 3.0$ (dotted line) and $V_0 = 4.5$ (dashed line).

In Figure 3 we show a plot of $P_1(\alpha_{eff})$ for $V_0 = 2.6$ (continuous line), $V_0 = 3.0$ (dotted line) and $V_0 = 4.5$ (dashed line). Clearly for $V_0 \leq 2.6$ it is most probable that there is no coherent discontinuity on the map ($\alpha_{eff}^{max} = 0$) with $P_1(\alpha_{eff} = 0) = 0.33$. On the other hand for $V_0 = 3.0$, the most probable value of α_{eff} is $|\alpha_{eff}^{max}| = 0.04$ with probability $P_1(\alpha_{eff}^{max}) \simeq 0.37$ while the probability that there is no coherent discontinuity on the map is $P_1(\alpha_{eff} = 0) \simeq 0.16$.

It is important to verify the above analytical results using Monte Carlo simulations of 2d data. We considered 2d 30×30 data-sets as described in section 3 with uncorrelated standardized Gaussian data (white noise). On these we superpose a coherent discontinuity with amplitude 2α with α in the range $[0, 0.45]$. For each α we construct 10 maps and find V_0 and its standard deviation $\sigma(V_0)$. We also find $\sigma(Y_{k_0^-})$ which was practically constant at $\sigma(Y_{k_0^-}) \simeq 0.07$ as predicted analytically. With the input V_0 and $\sigma(Y_{k_0^-})$ we construct $P_1(\alpha_{eff})$ and find $|\alpha_{eff}^{max}|$, $P_1(\alpha_{eff}^{max})$ and $P_1(0)$. These results are shown in Table 5.

Table 5: he effectiveness of the MSD statistic considered in two dimensional maps with a flat spectrum of fluctuations (white noise). First column shows the magnitude of the coherent discontinuity superposed on the standardized Gaussian map and the fourth column shows the *derived* most probable value value of α_{eff} (the lower bound of α) based on the MSD statistic.

α	V_0	$\sigma(Y_{k_0^-})$	$ \alpha_{eff}^{max} $	$P_1(0)$	$P_1(\alpha_{eff}^{max})$
0.00	2.6 ± 0.5	0.07	0.0 ± 0.01	0.36	0.36
0.03	2.8 ± 0.6	0.07	0.02 ± 0.02	0.31	0.37
0.06	3.4 ± 0.7	0.07	0.04 ± 0.02	0.06	0.37
0.1	4.1 ± 0.7	0.07	0.06 ± 0.03	0.005	0.37
0.2	5.6 ± 0.7	0.07	0.11 ± 0.03	0.0	0.37
0.25	7.5 ± 0.7	0.07	0.18 ± 0.03	0.0	0.37
0.3	9.0 ± 0.9	0.07	0.24 ± 0.03	0.0	0.37
0.35	9.8 ± 0.8	0.07	0.27 ± 0.03	0.0	0.37
0.4	10.4 ± 1.1	0.07	0.29 ± 0.03	0.0	0.37
0.45	12.4 ± 1.6	0.07	0.36 ± 0.04	0.0	0.37

Comparing α_{eff} with α we confirm that in all simulated cases $|\alpha_{eff}^{max}|$ is a lower bound on $|\alpha|$. It is also clear from Table 5 that the MSD method can detect the presence of a coherent discontinuity with $\alpha \gtrsim 0.04$ with probability ratio

$$\frac{P_1(\alpha_{eff} = 0.04)}{P_1(\alpha_{eff} = 0)} \simeq 7 \quad (53)$$

The MSD statistic is significantly more sensitive in detecting coherent discontinuities compared to the SMD statistic of sections 2, 3. We expect however that the sensitivity of this statistic will be significantly reduced when correlations are introduced in the data. We have shown using additional Monte-Carlo simulations that this

statistic is not as robust as the SMD statistic. In particular when we include correlations in the data (*e.g.* scale invariance), the sensitivity of the MSD statistic drops rapidly to the level of the SMD statistic *i.e.* it can detect a coherent discontinuity with $\alpha \gtrsim 0.4$. This implies that the MSD statistic is more useful in detecting the presence of coherent discontinuities only when applied to noise dominated data.

V. CONCLUDING REMARKS

An important issue that needs to be clarified is the following: 'What are the effects of other strings giving rise to their own step discontinuity? Do they decrease the sensitivity of the suggested statistical tests?'

No attempt is made in this paper to model the fluctuations of 'other strings'. Any such attempt (even those of simulations) is faced with the possibility of serious errors due to incorrect assumptions. Even basic features of the string scaling solution are still under serious debate. For example there have been serious claims recently [21] that realistic field theoretical cosmological simulations of gauged string evolution would have no wiggles for long strings and no loop component. In addition, the physical processes affecting the CMB photons are not well known especially in defect based models. The issues of reionization, fluctuations present on the last scattering surface, wiggles of long strings and other effects have only been crudely modeled so far.

Instead of attempting a rough modeling of these effects we have made a very robust and reasonable assumption: The statistics of CMB fluctuations induced by a string network on large angular scales are either gaussian (as was the common belief so far) or minimally non-gaussian in the sense that the only non-gaussianity is due to a late long string. Additional types of non-gaussianity are not excluded but they would simply make the detection of non-gaussianity easier by using the proposed (or other) tests. In that sense the proposed tests would only be able to find a lower bound on $G\mu$ which however turns out to be cosmologically quite interesting given the optimum sensitivity of the tests for detecting the above defined 'minimal non-gaussianity'.

The question that has been addressed in this paper is the following: Given the presently known values for $\frac{\delta T}{T}_{rms}$ from COBE on large angular scales, what is the minimum value of $G\mu$ detectable under the above stated assumption of 'minimal non-gaussianity'? Using the SMD or MSD statistics which are optimized to detect coherent temperature discontinuities on top of Gaussian temperature maps we may obtain non-trivial upper or even *lower* bounds on the values of $G\mu\nu_s\gamma_s$ which are

highly robust and independent of the details of the string evolution and the resolution of the CMB maps. Application of these statistics on the COBE data is currently in progress [19].

ACKNOWLEDGMENTS

I wish to thank N. Simatos and T. Tomaras for interesting discussions and for providing helpful comments after reading the paper. This work is the result of a network supported by the European Science Foundation. The European Science Foundation acts as catalyst for the development of science by bringing together leading scientists and funding agencies to debate, plan and implement pan-European initiatives. This work was also supported by the EU grant CHRX-CT94-0621 as well as by the Greek General Secretariat of Research and Technology grant IIENE Δ 95-1759.

-
- [1] . Guth & S. Pi, Phys.Rev.Lett. 49, 110 (1982);
S. Hawking, Phys.Lett. 115B, 295 (1982);
J. Bardeen, P. Steinhardt & M.Turner, Phys.Rev. D28, 679 (1983);
. Starobinsky, Phys.Lett. 117B, 175 (1982).
- [2] . W. B. Kibble, J.Phys. A9, 1387 (1976);
. Vilenkin, Phys.Rep. 121, 263 (1985);
. Vilenkin & . P. S. Shellard, 'Cosmic Strings and Other Topological Defects', Cambridge U. Press (1994);
R. Brandenberger, 'Topological Defect Models of Structure Formation After the COBE Discovery of CMB Anisotropies', Brown preprint BROWN-HET-881 (1992), publ. in proc. of the International School of Astrophysics "D.Chalonge", 6-13 Sept.1992;
L. Perivolaropoulos, Trieste HEP Cosmology, 204-270 (1994).
- [3] . Vilenkin, Phys.Rev. D23, 852 (1981).
- [4] . Turok, Phys. Rev. Lett. 63, 2625 (1989).
- [5] R. R. Caldwell, R. A. Battye & . P. S. Shellard, Phys. Rev. D54, 7146 (1996).
- [6] . Vachaspati, Phys. Rev. Lett. 57, 1655 (1986);
. Stebbins *et. al.*, Ap. J. 322, 1 (1987);
L. Perivolaropoulos, R. Brandenberger & A. Stebbins, Phys.Rev. D41, 1764 (1990);
. Vachaspati & . Vilenkin Phys. Rev. Lett. 67, 1057 (1991);
D. N. Vollick, Phys. Rev. D45, 1884 (1992);
. Hara & S. Miyoshi, Ap. J. 405, 419 (1993).
- [7] R. Brandenberger, N. Kaiser, E. P. S. Shellard, N. Turok, Phys.Rev. D36, 335 (1987).
- [8] . Vachaspati, Phys. Rev. D45, 3487 (1992).
- [9] . Vachaspati, Phys.Lett. B282, 305 (1992);
L. Perivolaropoulos & . Vachaspati, Ap. J. Lett. 423, L77 (1994).
- [10] F. R. Bouchet, D. P. Bennett & . Stebbins, Nature 335, 410 (1988);
D. Bennett, . Stebbins & F. Bouchet, Ap.J.(Lett.) 399, L5 (1992);
B. Allen, R.R. Caldwell, S. Dodelson, L. Knox, E.P.S. Shellard, A. Stebbins, Phys.Rev.Lett. 79, (1997).
- [11] J. Gott *et. al.* 1990, Ap.J. 352, 1 (1990);
L. Perivolaropoulos, Phys. Rev. D48, 1530 (1993);
R. Moessner, L. Perivolaropoulos & R. Brandenberger, Ap. J. 425,365 (1994);
J. Magueijo, Phys.Rev. D52, 4361 (1995);
X. Luo, Phys. Rev. D49, 3810 (1994);
D. Coulson, P. Ferreira, P. Graham & N. Turok, Nature, 368, 27 (1994).
- [12] G. Smoot *et. al.*, Ap. J. Lett. 396, L1 (1992);
E. L. Wright *et. al.*, Ap. J. Lett. 396, L5 (1992).
- [13] D. Scott, J. Silk & M. White, Science 268, 829 (1995);
PLANCK 1998, Homepage:
<http://astro.estec.esa.nl/SA-general/Projects/Planck/planck.html>;
MAP 1998, Homepage: <http://map.gsfc.nasa.gov>.
- [14] S. Veeraraghavan & A. Stebbins, Ap.J. 365, 37 (1990);
. Stebbins, Ap.J. 327, 584 (1988);
R. Brandenberger & . Turok, Phys. Rev. D33, 2182 (1986);
L. Perivolaropoulos, Phys.Lett. B298, 305 (1993).
- [15] N. Kaiser & . Stebbins, Nature 310, 391 (1984);
R. Gott, Ap. J. 288, 422 (1985).
- [16] D. Bennett & F. Bouchet, Phys.Rev.Lett. 60, 257 (1988);
. Albrecht & . Stebbins, Phys. Rev. Lett. 69, 2615 (1993);
. Allen & . P. S. Shellard, Phys.Rev.Lett. 64, 119 (1990).
- [17] B. Allen, R. Caldwell, E. P. S. Shellard, . Stebbins & S. Veeraraghavan, DAMTP R96/23, FERMILAB-Pub-96/265-A, WISC-MILW-96/21, astro-ph/9609038 (1996);
L. Perivolaropoulos, M.N.R.A.S., 267 529 (1993).
- [18] . Gangui, Phys. Rev. D54, 4750 (1996);
J. Magueijo, Phys.Rev. D52, 689 (1995).
- [19] Perivolaropoulos L. & Simatos N. 1998, in preparation.
- [20] S. Wolfram, *Mathematica version 3.0*, Addison-Wesley (1996).
- [21] G. Vincent, M. Hindmarsh & M. Sakelariadou, Phys. Rev. D56, 637 (1997).